JACS
JOURNAL OF THE AMERICAN CHEMICAL SOCIETY

Communication

pubs.acs.org/JACS

Mechanically Shaped Two-Dimensional Covalent Organic Frameworks Reveal Crystallographic Alignment and Fast Li-Ion Conductivity

Demetrius A. Vazquez-Molina,[†] Gavin S. Mohammad-Pour,[†] Chain Lee,[‡] Matthew W. Logan,[†] Xiangfeng Duan,[‡] James K. Harper,[†] and Fernando J. Uribe-Romo*[,†]

[†]Department of Chemistry, University of Central Florida, 4111 Libra Drive, Orlando, Florida 32816, United States

[‡]Department of Chemistry and Biochemistry, University of California—Los Angeles, 607 Charles E. Young Drive East, Los Angeles, California 90095, United States

Supporting Information

ABSTRACT: Covalent organic frameworks (COFs) usually crystallize as insoluble powders, and their processing for suitable devices is thought to be limited. We demonstrate that COFs can be mechanically pressed into shaped objects having anisotropic ordering with preferred orientation between *hk*0 and 00*l* crystallographic planes. Five COFs with different functionality and symmetry exhibited similar crystallographic behavior and remarkable stability, indicating the generality of this processing. Pellets prepared from bulk COF powders impregnated with $LiClO_4$ displayed room temperature conductivity up to 0.26 mS cm^{-1} and high electrochemical stability. This outcome portends use of COFs as solid-state electrolytes in batteries.

Covalent organic frameworks (COFs)[1] are increasingly interesting in materials chemistry due to their potential application in photovoltaics,[2] electrochemical devices,[3] and gas storage.[4] Two-dimensional (2D) COFs typically crystallize as stacked sheets that precipitate as insoluble powders, assumed to be unprocessable.[5] Cylindrical shape, narrow pore system size, and chemical stability make 2D COFs ideal candidates for applications where unidirectional mass transport is desired, such as transport of ions under electrochemical potentials. We explored the crystallographic and ionic transport features of 2D COF powders that were mechanically pressed into pellets with a high degree of crystallographic anisotropy. We demonstrate that this method could be applied to different COFs with diverse functionalities (boronate, boroxine, β-ketoenamine, triazine) and symmetries (hexagonal and tetragonal) and used to prepare COFs for large devices, such as solid-state fast-ion conductors for Li ions. Highly aligned porous 2D COFs can be specifically tailored to conduct Li ions at ultrafast rates for use as electrolytes in all-solid-state batteries.

Thin films of 2D COFs can be prepared by either addition of flat substrates to the crystallizing mixture[6] or mechanical delamination of powders[7] and obtained as highly aligned 200 nm thick samples. Preparation of macroscopic COF samples with crystallographic alignment for large devices has not been realized.[8] We hypothesized that the weak $\pi-\pi$ interaction between the layers of the COF allows easy slipping under mechanical stress, allowing an anisotropic packing of the crystallites, similar to graphite. We used the archetypical COF-5,[1a] which packs in a hexagonal crystal system with two degrees of freedom: $a = b$ and c (Figure 1a), where the covalently bound sheets lay along ab (Figure 1a, green arrows) and stack along c (Figure 1a, blue arrow) through $\pi-\pi$ interactions. This hexagonal

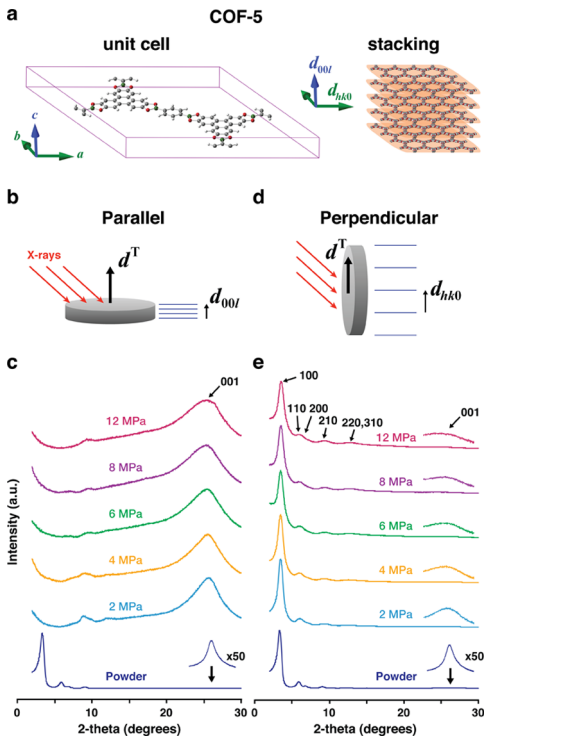

Figure 1. (a) Unit cell of COF-5 illustrating the stacking and orthogonality between d_{hk0} and d_{00l} plane normal vectors. (b) COF pellet oriented parallel to the optical axis. (c) PXRD of a COF-5 pellet in *parallel* mode at varying uniaxial pressure. (d) COF pellet oriented perpendicular to the optical axis. (e) PXRD of a COF-5 pellet in *perpendicular* mode at varying uniaxial pressure. The 001 peak is shown in the inset and is expanded 50 times for clarity; d^T corresponds to the optical axis normal vector and d_{hkl} to the *hkl* plane normal vector.

Received: May 31, 2016
Published: July 14, 2016

DOI: 10.1021/jacs.6b05568
J. Am. Chem. Soc. 2016, 138, 9767−9770

packing allows for two sets of Bragg planes: *hk*0 and 00*l*, which are orthogonal to each other and are the signature for any anisotropy in the diffraction pattern. We prepared bulk powders of the COF, and a typical powder X-ray diffraction (PXRD) pattern of the fully isotropic powder is shown in Figure 1c,e (dark blue trace). When samples of the COF powder were pressed into pellets using a uniaxial hydraulic press, an apparent loss of crystallinity was observed when the diffractogram was measured with the pellet resting on its round side parallel to the optical axis (Figure 1b, hereafter *parallel* mode), which is also parallel to the uniaxial press at increasing uniaxial pressure (Figure 1c). Surprisingly, the broad diffraction peak at 26° 2θ, which corresponds to the 001 Bragg reflection, was predominantly observed when the pellet was pressed >12 MPa. Turning the pellet 90°—resting on its edge (Figure 1d, hereafter *perpendicular* mode)—resulted in a pattern that displayed the expected low-angle *hk*0 peaks in COF-5 (Figure 1e). Moreover, the intensity of the 001 peak decreased with increasing uniaxial pressure (Figure 1e, inset). According to Bragg theory,[9] to observe diffraction in an isotropic powder, the d_{hkl} normal vector must be parallel to the optical axis normal vector, d^{T} (Figure 1b), in which all Bragg planes fulfill this condition. This is the case for the 00*l* planes (along the *c* axis) in *parallel* mode but not for the *hk*0 (along the *ab* axis). If these *hk*0 planes are aligned perpendicular to d^{T}, they will not diffract. When the pellet is aligned in *perpendicular* mode, the d_{hkl} vector of the *hk*0 planes are aligned with the d^{T} and are therefore able to diffract. This suggests that there is an anisotropic orientation induced by mechanical pressing, where the 00*l* planes are the only ones that fulfill the diffraction condition when the pellet is in *parallel* mode and the *hk*0 planes when the pellet is in *perpendicular* mode. This behavior is known in powder diffractometry as preferred orientation and is observed in large crystals with a very anisotropic crystallite shape[10] and in thin films.[11]

This pressure-induced crystallographic preferred orientation was observed in other 2D materials that stack through van der Waals interactions, but only in inorganic materials at very high pressures.[12] However, this is the first time it is measured in organic porous framework materials. Preferred orientation in COFs is a very attractive feature because inducing alignment will result in alignment of the cylindrical pores. We hypothesized this phenomenon is inherent in all layered 2D COFs; therefore, we explored the effect of uniaxial pressing in other 2D COF bulk powders with different functionality and crystal symmetry. Powder samples of hexagonal COF-1 (boroxine),[1a] TpPa-1 COF (β-ketoenamine),[13] CTF-1 (triazine),[14] and tetragonal ZnPc-BBA COF (boronate)[15] were pressed into pellets and crystallographic behavior similar to that in COF-5 was observed. All four COFs displayed the expected preferred orientation (Figure 2). When the pellets were in *parallel* mode, all COFs displayed an intensity increase along the 001 reflection (002 for COF-1) and attenuation of the 100 peaks. In COF-1, some residual intensity was observed in the 110 reflections; however, the intensity of the 002 peak is significantly enhanced, and even some non-orthogonal *h*0*l* reflections remain (such as 101 and 201), consistent with their alignment with respect to the optical axis. In *perpendicular* mode, all COFs displayed the corresponding *hk*0 peaks with attenuation of the 00*l* reflections. COF-1 displayed an obvious difference in peak width. This peak width is a result of anisotropic crystallite size and strain. A negative control was performed by pressing a 3D COF (COF-102[16]) into a pellet, where a complete loss of crystallinity was observed in either pellet orientation, suggesting that only 2D COFs exhibit this property.

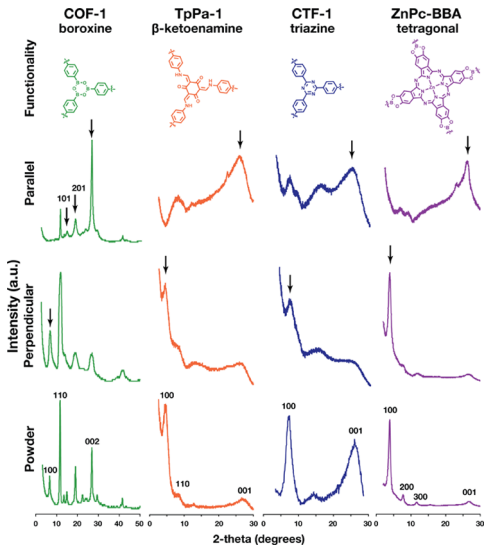

Figure 2. PXRD patterns of COFs with multiple functionality (top) in powder (bottom) and pellets in both orientations (middle). Pellets pressed at 12 MPa (CTF-1 pressed at 15 MPa). Preferred orientation of the 100 and 001 (002 for COF-1) reflections is indicated with arrows.

Grinding a pellet into a powder resulted in complete recovery of the diffraction peaks (Figure 3a), indicating the stability of the COF under mechanical stress. As noted in Figure 1c,e, gradual broadening of the diffraction peaks was observed with increasing uniaxial pressure and after regrinding the pellets. Le Bail refinement of the diffraction patterns elucidated the crystalline domain size and strain present in the powder, pellets, and ground pellet along the *ab* and *c* unit cell directions (Figure 3b).[17] Pressing the COF-5 powder into a pellet decreases the crystalline domain size by 75%, but only along *ab*, with no significant change along *c*. This decrease in size is independent of applied pressure, and domain size is preserved after grinding a pellet pressed at 12 MPa. The most interesting feature is the change in crystalline strain. A gradual increase in strain is observed along both directions with increasing uniaxial pressure, up to ~25% along *c* at 12 MPa; this strain arises from deviations in the interplanar distances of the sheets due to applied mechanical stress. This strain is relieved when the pellet is ground back into a powder and is an important trait that could affect the mechanical properties and performance of 2D COFs. Morphological changes of the COFs at the mesoscopic scale were also followed via SEM, where

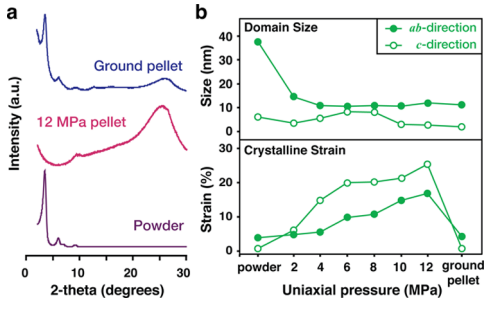

Figure 3. (a) PXRD of COF-5 as powder before mechanical pressing (purple), as pellet in *parallel* mode (red) and after grinding of the pellet (blue), indicating the crystalline stability after mechanical stress. (b) Crystalline domain size and strain of COF-5 at varying uniaxial pressures, as determined from line width analysis using Le Bail refinement, showing the effects of the mechanical stress.[17]

DOI: 10.1021/jacs.6b05568
J. Am. Chem. Soc. 2016, 138, 9767–9770

a drastic change in sample morphology was observed. COF samples change their particle shape from globular agglomerates of COF crystallites in the powder (Figure S31) to highly anisotropic sheet-like features in the pellet (Figure S32). The sheets are perpendicular to the compression, supporting the crystallographic preferred orientation.

This alignment will make COFs applicable where pore orientation is vital (i.e., in the transport of charged species in electrochemical devices). This is the case because the pore of the COF is constrained by the arrangement of layers in the unit cell; any alignment of the COF unit cell induces change in pore orientation. The effect of the mass transfer within the pores of the compressed COFs was studied to provide insight into the alignment of the cylindrical pores, more specifically, with ionic transfer, thus exploring the applicability of COFs as solid-state electrolytes for use in safer and more efficient all-solid-state Li-ion batteries.[18] COFs have been utilized as solid electrolytes for proton conduction;[17] however, there are only a few studies on conductivity of larger cations in organic frameworks. Powders of COF-5 and TpPa-1 COFs were immersed in 1 M $LiClO_4$/THF for 48 h to impregnate the Li salt into the COF, with observed loading of 3.77 mol % Li^+ to COF (i.e., based on B/Li ratio) from elemental analysis.[19] Evaporation of excess solvent after removal from the Li solution by filtration and thorough rinse provided dry COF powder that was pressed into pellets under 4 MPa uniaxial pressures. EIS was performed on the pellets of $LiClO_4$-impregnated COFs to study their use as solid-state electrolytes for Li-ion batteries.[17] In both cases, a Nyquist behavior was observed (Figure 4a), where the plot of the real component (Z') versus the imaginary component (Z'') of the complex impedance function displays a semicircular shape followed by a spike.[20] Conductivity of the solid electrolyte can be determined from this plot, where the resistance of the electrolyte is the real component of the impedance at high frequencies, resulting in ionic conductivities of $\sigma = 0.26$ and 0.15 mS cm^{-1} for COF-5 (Figure 4a) and TpPa-1 (Figure S25), respectively, at room temperature. Pellets of nonimpregnated COFs displayed no Nyquist behavior, indicating that the conductivity observed is due to $LiClO_4$ in the material. Variable-temperature studies on the COF-5 pellet allowed bulk activation energy to be determined for ionic conductivity (E_a) using a linear Arrhenius plot (Figure 4b), with $E_a = 37 \pm 4$ meV. Conductivity is within the recommended range for actual devices[21] and competitive with other materials such as a spiroborate-based COF ($\sigma = 0.03$ mS cm^{-1}),[22] borate amorphous organic porous polymers ($\sigma = 0.27$ mS cm^{-1}),[23] metal–organic frameworks ($\sigma = 0.31$ mS cm^{-1}),[24] and other inorganic materials such as LiPON and LiGePS ($\sigma = 8.8 \times 10^{-4}$ to 12.0 mS cm^{-1}) at room temperature.[25] Note that E_a of $LiClO_4$-impregnated COF-5 is significantly smaller than that of the previously mentioned materials, which implies that the conductivity is less dependent on the temperature in the measured range. Compared to highly conducting LiGePS ceramics, COFs offer more versatile synthesis under milder conditions.

Electrochemical stability of the $LiClO_4$-impregnated COF-5 pellet was measured in an asymmetric two-electrode Li| $LiClO_4$(COF-5)|steel cell utilizing cyclic voltammetry (CV).[17] Besides a small amount of Li deposition/dissolution at negative potentials, the CV displays a featureless trace between −1.0 and 10. V vs Li^+/Li^0 (Figure S26) up to 100 cycles, surpassing the stability observed in the LiGePS ceramics.[26] High ionic conductivity, low temperature, and high electrochemical stability make COF-5 a competitive candidate for solid electrolytes in rechargeable Li-ion batteries.

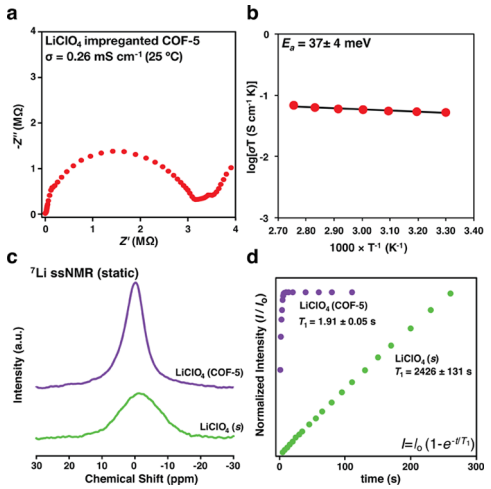

Figure 4. Complex impedance function (a) and Arrhenius plot (b) of COF-5 impregnated with $LiClO_4$; conductivity at room temperature and activation energy are indicated. (c) Static ^{7}Li ssNMR spectra of COF-5 impregnated with $LiClO_4$ (purple), compared to pure $LiClO_4$ (green). (d) Saturation recovery plot from ^{7}Li ssNMR spectra (7 kHz, magic angle spinning) of COF-5 impregnated with $LiClO_4$ (purple) vs pure $LiClO_4$ (green). T_1 relaxation time constant in each material reveals the differences in mobility of the ^{7}Li ions.[17]

To further evaluate the dynamic behavior of Li^+ within the COF, we measured the ^{7}Li static solid-state nuclear magnetic resonance (ssNMR) spectrum of the $LiClO_4$-impregnated COF-5 (powder) compared to $LiClO_4$(s). Figure 4c displays the spectrum of solid $LiClO_4$ (green) to illustrate the spectroscopic behavior of Li^+ in a solid matrix with very limited mobility. A broad signal is observed in the spectrum as a result of solid-state dipole–dipole and quadrupolar couplings between ^{7}Li sites. Determination of the T_1 relaxation time of $LiClO_4$ by saturation–recovery pulse sequence with magic angle spinning (Figure 4d) resulted in a $T_1 = 2426 \pm 131$ s. This large value is commensurate with very nonmobile ^{7}Li species, as expected for a nonconducting solid salt.[26] The presence of more mobile ^{7}Li species results in diminishing the effect of the solid-state couplings, yielding narrow ^{7}Li NMR signals as observed in the $LiClO_4$-impregnated COF-5 (Figure 4c, purple) compared to solid $LiClO_4$. Saturation recovery experiments resulted in relaxation times of $T_1 = 1.91 \pm 0.05$ s, about 4 orders of magnitude smaller than that in solid perchlorate salt. The presence of sharper signals and much smaller T_1 shows dynamic behavior of the Li^+ cation in solid COF, implying high ionic mobility within. A crucial question regarding $LiClO_4$-impregnated COF-5 is whether the Li is located within the pores or bound to the surface. Isotropic ^{7}Li MAS NMR spectrum of Li-treated COF-5 exhibits only a single resonance (Figure S41), indicating the presence of only one environment for ^{7}Li. Previously described T_1 measurements indicate that this environment is highly mobile. These results are inconsistent with rigidly bound surface Li and imply that $LiClO_4$ is located within the pores.

Another question that remains is the effect of mechanical treatment on the porosity of the materials. Pressing COF-5 into pellets results in samples that exhibit no porous behavior to N_2 gas. Mechanical processing[7a] in COFs results in decrease or loss of porous behavior, an effect of the disturbance of a long-range pore structure due to the sliding of layers. There is a slow diffusion effect of the N_2 into the pellet due to the limited gas accessibility to the pores arising from the mechanical pressing. Impregnation

DOI: 10.1021/jacs.6b05568
J. Am. Chem. Soc. 2016, 138, 9767–9770

of the COF powder with $LiClO_4$ before mechanical processing results in the isotherm shape and pore size distribution of COF-5 but with much less absolute uptake (~7%, Figures S27–S30),[17] indicating effective impregnation of the Li salt within the COF, as the salt clogs the pores and increases the effective mass. Once the COF is impregnated, apparent loss of porosity to gas is inconsequential to Li^+ conduction. Immersion of a non-impregnated COF-5 pellet in 1 M $LiClO_4$/THF results in no Nyquist behavior. In fact, such pellets rapidly return to powder form. Thus, impregnation of the COF with Li salts is vital while still porous, before the mechanical processing.

We determined that pressing 2D COF powders into pellets for device fabrication in solid-state electrolytes results in an anisotropic crystallographic ordering of the sheets. We studied the effect of the uniaxial pressure on the alignment and domain size of the crystallites, elucidating the structural stability of the prepared COFs even after regrinding the pellets. We observed that this crystallographic alignment is a property applicable to 2D COFs of different molecular functionality and crystallographic symmetry, that the crystallographically aligned materials display fast Li-ion conductivity and dynamics within the COFs and exceptional electrochemical stability to Li. Further efforts to study Li-ion mobility, formation of passivation layers, Li^+ transport number, and incorporation into battery assemblies are currently ongoing.

■ ASSOCIATED CONTENT

Supporting Information

The Supporting Information is available free of charge on the ACS Publications website at DOI: 10.1021/jacs.6b05568.

Materials and methods, synthesis and mechanical pressing procedures, crystallographic and electrochemical procedures, and further data analysis (PDF)

■ AUTHOR INFORMATION

Corresponding Author

*fernando@ucf.edu

Notes

The authors declare no competing financial interest.

■ ACKNOWLEDGMENTS

We thank the University of Central Florida College of Sciences for startup funds, Mr. Richard Zotti (UCF CREOL) for technical assistance, Prof. Mark Orazem (U. of Florida), and Prof. Joaquin Rodríguez-López and Dr. Kenneth Hernandez-Burgos (U. of Illinois Urbana—Champaign) for helpful discussions. This work was supported by the National Science Foundation under CHE-1255159 to J.K.H.

■ REFERENCES

(1) (a) Côté, A. P.; Benin, A. I.; Ockwig, N. W.; Matzger, A. J.; O'Keeffe, M.; Yaghi, O. M. *Science* **2005**, *310*, 1166–1170. (b) Colson, J. W.; Dichtel, W. R. *Nat. Chem.* **2013**, *5*, 453–465. (c) Waller, P. J.; Gándara, F.; Yaghi, O. M. *Acc. Chem. Res.* **2015**, *48*, 3053–3063.

(2) (a) Wan, S.; et al. *Chem. Mater.* **2011**, *23*, 4094–4097. (b) Dogru, M.; Handloser, M.; Auras, F.; Kunz, T.; Medina, D.; Hartschuh, A.; Knochel, P.; Bein, T. *Angew. Chem., Int. Ed.* **2013**, *52*, 2920–2924. (c) Dogru, M.; Bein, T. *Chem. Commun.* **2014**, *50*, 5531–5546. (d) Chen, C.-P.; Huang, C.-Y.; Chuang, S.-C. *Adv. Funct. Mater.* **2015**, *25*, 207–213.

(3) (a) DeBlase, C. R.; Silberstein, K. E.; Truong, T.-T.; Abruña, H. D.; Dichtel, W. R. *J. Am. Chem. Soc.* **2013**, *135*, 16821–16824. (b) DeBlase, C. R.; Hernández-Burgos, K.; Silberstein, K. E.; Rodríguez-Calero, G. G.; Bisbey, R. P.; Abruña, H. D.; Dichtel, W. R. *ACS Nano* **2015**, *9*, 3178–3183. (c) Yang, H.; et al. *ACS Appl. Mater. Interfaces* **2016**, *8*, 5366–5375. (d) Xu, F.; Jin, S.; Zhong, H.; Wu, D.; Yang, X.; Chen, X.; Wei, H.; Fu, R.; Jiang, D. *Sci. Rep.* **2015**, *5*, 8225. (e) Liao, H.; Ding, H.; Li, B.; Ai, X.; Wang, C. *J. Mater. Chem. A* **2014**, *2*, 8854–8858. (f) Liao, H.; Wang, H.; Ding, H.; Meng, X.; Xu, H.; Wang, B.; Ai, X.; Wang, C. *J. Mater. Chem. A* **2016**, *4*, 7416–7421.

(4) Doonan, C. J.; Tranchemontagne, D. J.; Glover, T. G.; Hunt, J. R.; Yaghi, O. M. *Nat. Chem.* **2010**, *2*, 235–238.

(5) Sakamoto, J.; van Heijst, J.; Lukin, O.; Schlüter, A. D. *Angew. Chem., Int. Ed.* **2009**, *48*, 1030–1069.

(6) (a) Colson, J. W.; Woll, A. R.; Mukherjee, A.; Levendorf, M. P.; Spitler, E. L.; Shields, V. B.; Spencer, M. G.; Park, J.; Dichtel, W. R. *Science* **2011**, *332*, 228–231. (b) Spitler, E. L.; Koo, B. T.; Novotney, J. L.; Colson, J. W.; Uribe-Romo, F. J.; Gutierrez, G. D.; Clancy, P.; Dichtel, W. R. *J. Am. Chem. Soc.* **2011**, *133*, 19416–19421. (c) Spitler, E. L.; Colson, J. W.; Uribe-Romo, F. J.; Woll, A. R.; Giovino, M. R.; Saldivar, A.; Dichtel, W. R. *Angew. Chem., Int. Ed.* **2012**, *51*, 2623–2627.

(7) (a) Chandra, S.; Kandambeth, S.; Biswal, B. P.; Lukose, B.; Kunjir, S. M.; Chaudhary, M.; Babarao, R.; Heine, T.; Banerjee, R. *J. Am. Chem. Soc.* **2013**, *135*, 17853–17861. (b) Bunck, D. N.; Dichtel, W. R. *J. Am. Chem. Soc.* **2013**, *135*, 14952–14955.

(8) Pellets of COFs were prepared, but no crystallographic measurements were performed. See refs 3d, 4, 18, and 23.

(9) Pecharsky, V. K.; Zavalij, P. Y. *Fundamentals of Powder Diffraction and Structural Characterization of Materials*, 2nd ed.; Springer: New York, 2009.

(10) Manson, J. E. *J. Appl. Phys.* **1955**, *26*, 1254–1256.

(11) Vaudin, M. D. *J. Res. Natl. Inst. Stand. Technol.* **2011**, *106*, 1063–1069.

(12) (a) Zhao, Y. X.; Spain, I. L. *Phys. Rev. B: Condens. Matter Mater. Phys.* **1989**, *40*, 993–997. (b) Bandaru, N.; et al. *J. Phys. Chem. C* **2014**, *118*, 3230–3235.

(13) Kandambeth, S.; Mallick, A.; Lukose, B.; Mane, M. V.; Heine, T.; Banerjee, R. *J. Am. Chem. Soc.* **2012**, *134*, 19524–19527.

(14) Kuhn, P.; Antonietti, M.; Thomas, A. *Angew. Chem., Int. Ed.* **2008**, *47*, 3450–3453.

(15) Colson, J. W.; Mann, J. A.; DeBlase, C. R.; Dichtel, W. R. *J. Polym. Sci., Part A: Polym. Chem.* **2015**, *53*, 378–384.

(16) El-Kaderi, H. M.; Hunt, J. R.; Mendoza-Cortés, J. L.; Côté, A. P.; Taylor, R. E.; O'Keeffe, M.; Yaghi, O. M. *Science* **2007**, *316*, 268–272.

(17) See Supporting Information for experimental details.

(18) Kalhoff, J.; Eshetu, G. G.; Bresser, D.; Passerini, S. *ChemSusChem* **2015**, *8*, 2154–2175.

(19) (a) Chandra, S.; Kundu, T.; Kandambeth, S.; BabaRao, R.; Marathe, Y.; Kunjir, S. M.; Banerjee, R. *J. Am. Chem. Soc.* **2014**, *136*, 6570–73. (b) Shinde, D. B.; et al. *J. Mater. Chem. A* **2015**, *4*, 2682–2690. (c) Ma, H.; Liu, B.; Li, B.; Zhang, L.; Li, Y.-G.; Tan, H.-Q.; Zang, H.-Y.; Zhu, G. *J. Am. Chem. Soc.* **2016**, *138*, 5897–5903. (d) Xu, H.; Tao, S.; Jiang, D. *Nat. Mater.* **2016**, *15*, 722.

(20) Orazem, M. E.; Tribollet, B. *Electrochemical Impedance Spectroscopy*, 1st ed.; Wiley-Interscience: New York, 2008.

(21) Goodenough, J. B.; Kim, Y. *Chem. Mater.* **2010**, *22*, 587–603.

(22) Du, Y.; Yang, H.; Whiteley, J. M.; Wan, S.; Jin, Y.; Lee, S.-H.; Zhang, W. *Angew. Chem., Int. Ed.* **2016**, *55*, 1737–1741.

(23) Van Humbeck, J. F.; Aubrey, M. L.; Alsbaiee, A.; Ameloot, R.; Coates, G. W.; Dichtel, W. R.; Long, J. R. *Chem. Sci.* **2015**, *6*, 5499–5505.

(24) Wiers, B. M.; Foo, M.-L.; Balsara, N. P.; Long, J. R. *J. Am. Chem. Soc.* **2011**, *133*, 14522–14525.

(25) (a) Kamaya, N.; et al. *Nat. Mater.* **2011**, *10*, 682–686. (b) Bachman, J. C.; et al. *Chem. Rev.* **2016**, *116*, 140–162. (c) Senevirathne, K.; Day, C. S.; Gross, M. D.; Lachgar, A.; Holzwarth, N. A. W. *Solid State Ionics* **2013**, *233*, 95–101.

(26) Keller, J. *Understanding NMR Spectroscopy*, 2nd ed.; Wiley: Chichester, 2010.

DOI: 10.1021/jacs.6b05568
J. Am. Chem. Soc. 2016, 138, 9767–9770